



GRAND

Graphene-based Nanoelectronic Devices

Small or medium-scale focused research project

WP2 Fabrication & Material Characterization

Deliverable 2.4 “Report on graphene nanoanalytics”

Main Author(s):

UCAM: C. G. Smith, M. R. Connolly

Due date of deliverable: M24

Actual submission date: M24

Project funded by the European Commission under grant agreement n°215752

LIST OF CONTRIBUTORS

Partner	Acronym	Laboratory Name	Name of the contact
1 (coordinator)	AMO	Gesellschaft fuer angewandte Mikro- und Optoelektronik mit beschraenkter Haftung	Heinrich Kurz
2	IUNET	Consorzio Nazionale Interuniversitario per la Nanoelettronica	Enrico Sangiorgi
3	CEA-LETI	Commissariat à l'Energie Atomique	Thierry Poiroux
4	TNI-UCC	University College Cork, National University of Ireland, Cork, Tyndall National Institute	Aidan Quinn
5	UCAM DPHYS	University of Cambridge	Charles Smith
6	STM SAS	STMicronics (Crolles 2) SAS	Frederic Boeuf

TABLE OF CONTENTS

The deliverable must be 10 pages maximum (without references)

Deliverable Summary	4
I. LOCAL PROBES OF GRAPHENE	5
II. COMPARISON OF MAIN IMAGING TECHNIQUES.....	6
A. Scanning gate microscopy.....	6
B. Scanning tunneling microscopy	8
C. Electrostatic force microscopy.....	10
D. Raman	12
E. Other techniques	13
III. CONCLUSIONS	13
IV. REFERENCES.....	13

Deliverable Summary

Graphene's candidacy for spearheading semiconductor technology into the "Beyond CMOS" era is largely predicated on its extremely high carrier mobility ($>100 \text{ m}^2/\text{Vs}$) and gate tunable carrier density. Since these transport properties are fundamentally controlled by interactions between conduction electrons and the local environment of graphene, local probe experiments ("nanoanalytics") in particular are expected to yield key insights. Specifically within the GRAND framework, the objective of nanoanalytics is to understand transport properties, such as mobility and energy gaps, of graphene nanoribbons (GNRs) in terms of their underlying atomic and electronic structure. In this deliverable we review the progress we have made in this direction using scanning gate microscopy experiments on 2D flakes and GNRs. While GNRs are the core subject of our local probe experiments, 2D graphene flakes feature strongly as useful test-beds for chemical functionalization routines being developed by in collaboration with the other GRAND partners (AMO and TNI-UCC).

Ideally our study also provides experimental access to the influence of edge lattice symmetries, topographic features, surface adsorbates, as well as the local electrostatic environment of graphene's host substrate. To this end we also review techniques such as scanning tunneling microscopy (STM), electrostatic force microscopy (EFM), and Kelvin probe microscopy (KPM) which we envisage using in the near future. We show that STM will give us experimental access to edges states and energy gaps, while EFM and KPM will enable us to probe electrostatics at mesoscopic lengthscales. We believe the combined application of these techniques will have an impact on GRAND's objective to optimize the performance of graphene nanoribbon field effect devices (GNR-FEDs).

I. LOCAL PROBES OF GRAPHENE

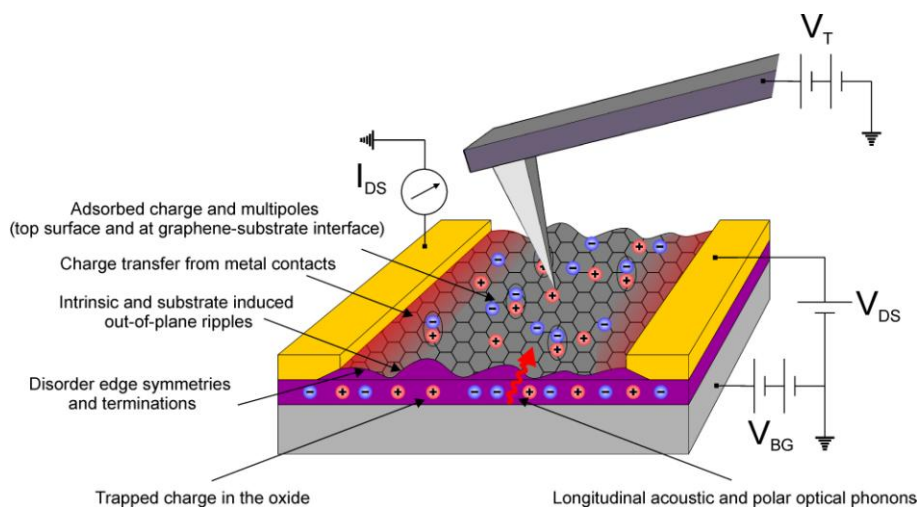


Figure 1: Schematic depiction of scanning probe experiment on graphene. Some of the tip-graphene and substrate-graphene interactions have been labelled to highlight the importance of spatially resolved measurements.

Before launching into more detail it is important to briefly outline what structures we expect to image in graphene. For simplicity we consider two distinct phenomena where spatially resolved measurements have or will make an impact: the origin of transport gaps in patterned 1D structures (GNRs in particular) and the mechanism limiting the mobility in supported 2D flakes. The first line of enquiry stems from graphene's unique gapless bandstructure, which in the presence of potential disorder leads to a minimum conductivity in the limit of vanishing carrier density. Without an insulating state, the "on/off" conductance modulation of graphene field effect devices is prohibitively low for some envisaged applications such as novel switches and FETs in logic applications. Over the last few years considerable effort has been devoted to introducing a transport gap through patterning graphene into one dimensional nanoribbons. It was indeed found that the conductance of GNRs can be made vanishingly small due to the opening up of a width-dependent confinement gap [27], but the size of the transport gap exceeds estimates based on lateral confinement effects alone and the gapped region is also full of sharp resonances [28,29]. Several mechanisms have been proposed to explain these observations including renormalized lateral confinement [27], Anderson localisation [17], percolation models [47] and disorder induced quantum dot formation [48]. The fact that these mechanisms are partly distinguished by *where* the localisation occurs makes the application of local probes particularly appealing. The second line of enquiry focuses on understanding why the mobility of supported 2-D graphene in real devices is usually only 0.1-20 m²/Vs, an order of magnitude less than needed to make graphene technologically competitive at room temperature. There is growing evidence to suggest that the mobility is limited by long-range scattering from charged impurities (CI) and out-of-plane ripples. Sources of CI include physi- and chemi-sorbed atmospheric gases [9,18,30], residue from tape used during exfoliation [7], monolayers of photo- or ebeam- resist (PMMA) left over from the microfabrication of electrical contacts [31], trapped charges in the substrate [18], and molecules such as H₂O trapped between the graphene and the SiO₂ [19]. Because the measured conductance of graphene will depend on the microscopic scattering processes

from each source of CI, spatially resolved measurements of CI densities and lengthscales are also expected to yield key insights in this area.

II. COMPARISON OF MAIN IMAGING TECHNIQUES

A. Scanning gate microscopy

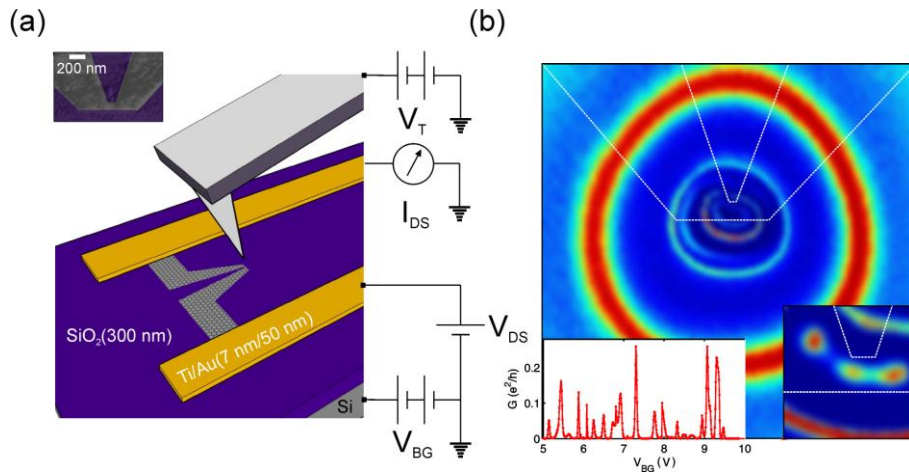
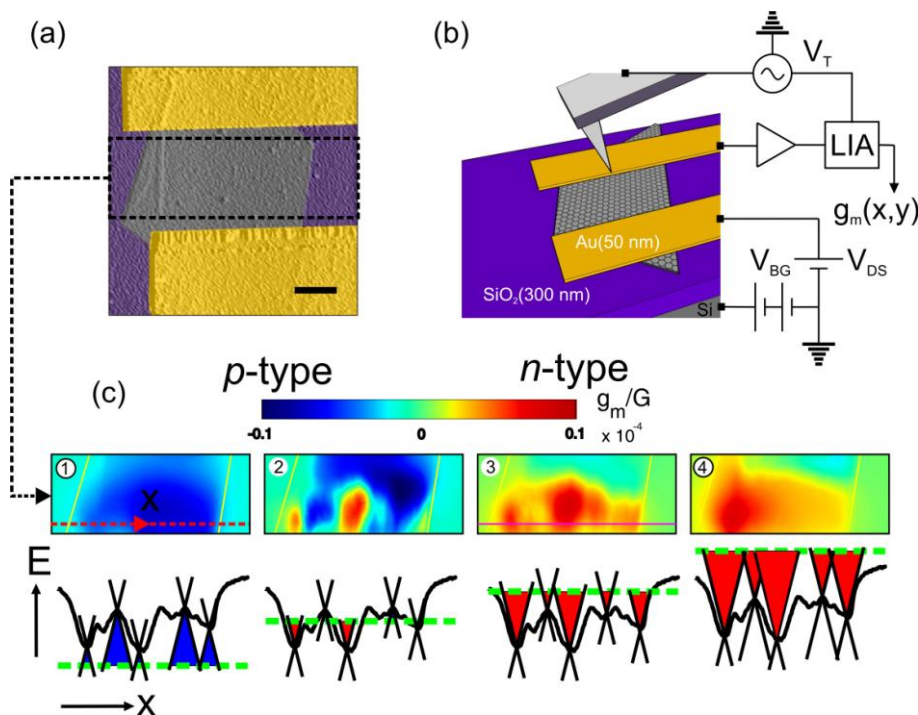


Figure 2. Scanning gate microscopy of GNRs. (a) Setup used to perform SGM. Inset: False-color atomic force micrograph of the 90 nm wide GNR. (b) SGM image ($2 \mu\text{m} \times 2 \mu\text{m}$) showing the conductance of the GNR as a function of tip position ($V_T = 2 \text{ V}$, $V_{BG} = 2 \text{ V}$). The white outline indicates the edge of the GNR. Inset (right): High resolution SGM image of the GNR ($0.4 \mu\text{m} \times 0.4 \mu\text{m}$). Inset (left): Zero-bias conductance of the GNR as a function of backgate voltage ($T = 8 \text{ K}$).

Scanning gate microscopy is a local probe technique commonly used to map spatial variations in the local conductivity of subsurface conducting systems such as two dimensional electron gases in semiconductor heterostructures. To perform SGM a DC current (I_{DS}) is driven through the sample and the perturbation of the bulk conductance due to the presence of a charged tip is recorded as a function of the tip position [Fig. 2(a)]. Regions which are sensitive to local electric fields, for example because the current density or field-effect mobility is high there, can be then be imaged with $\approx 50 \text{ nm}$ resolution. Surprisingly SGM has not been widely used to investigate graphene despite its high spatial resolution [5] owing to the somewhat poor signal-to-noise ratio (SNR) achievable at room temperature. The problem of poor SNR stems from the fact that the SGM signal depends on the relative area of the tip-perturbed region to the rest of the sample, which in micron-sized 2D systems such as graphene is obviously rather small ($\sim 10^{-4}$). Historically applications of SGM have thus focused on 0D and 1D samples (carbon nanotubes and semiconducting quantum dots) which exhibit large changes in conductance with tip position. We have recently used low temperature SGM to perturb the transport through a 90 nm wide graphene nanoribbon which, due to the increased sensitivity shown by 1D systems, exhibits strong conductance modulations with tip position. The SGM image shown in Fig. 2(b) typifies our latest results. The structure in these images can be understood by inspecting the conductance of the GNR as a function of back-gate voltage [inset, Fig.2(b)]. The conductance haloes [Fig. 2(b)] manifest whenever the potential from the tip at the GNR is sufficient to overcome the Coulomb blockade. The key result of this experiment is that the focus of the haloes is located *within* the GNR channel itself [inset, Fig.2 (b)], clearly demonstrating SGM's power to

discriminate between localisation mechanisms in GNRs. The longitudinal extent and shape of the halo features are also reminiscent of potential fluctuations imaged in the underlying oxide [9], supporting the theory that potential disorder drives the localisation. In our next experiment on micron-long GNRs, SGM will allow us to image isolated dots and estimate the density of tunnel barriers due, for example, to disordered edges or necking in etched devices manufactured by AMO.

We have also exploited a.c. detection techniques to improve the SNR of SGM on 2D graphene devices [Fig.3(a)]. To do this the potential difference V_T between the tip and the graphene is modulated at a low frequency (typically 3 V @ 1 kHz) and the corresponding modulation of the current through the flake is amplified ($\times 10^7$) and detected using a lock-in amplifier [Fig.3(b)]. The reference frequency is chosen to be low enough to avoid any mixing with the small potential modulation induced by the oscillation in the tip-sample height. A ≈ 250 μ A source-drain current is driven through the flake and the demodulated component of the current, proportional to the transconductance $g_m = dI/dV_T$, is recorded as a function of tip position. Figure 3(c) shows a series of $g_m(x,y)$ images captured at different back-gate voltages. As the back-gate voltage moves the Fermi level, domains in the flake emerge with different carrier densities, allowing one to map out the mobility and distribution of charged impurities (see ref.[4].) Note that in these experiments the cantilever is in intermittent contact with the graphene in order to preserve the shape of the tip and also to avoid any unintentional exchange of material between the probe and the graphene. In summary due to the success of SGM we envisage it becoming more prevalent in future studies, especially at low temperature



where non-local effects come into play.[5]

Figure.3: Transconductance scanning gate microscopy of 2D flakes. (a) False-color AFM image showing a contacted graphene flake (Scale bar 2 μ m.) (b) Setup used to perform AC scanning gate microscopy. (c) Raw SGM images showing the inhomogeneous transition from p-type to n-type conduction after current-annealing [4]. Images 1-4 are taken at $V_{BG} = -10$ V, 0 V, 6 V, 10 V, respectively. The Dirac point profile along the red dashed line (image 1)

is depicted beneath each picture together with the Dirac cone in energy-momentum space. The green dashed line represents the position of the Fermi level.

B. Scanning tunneling microscopy

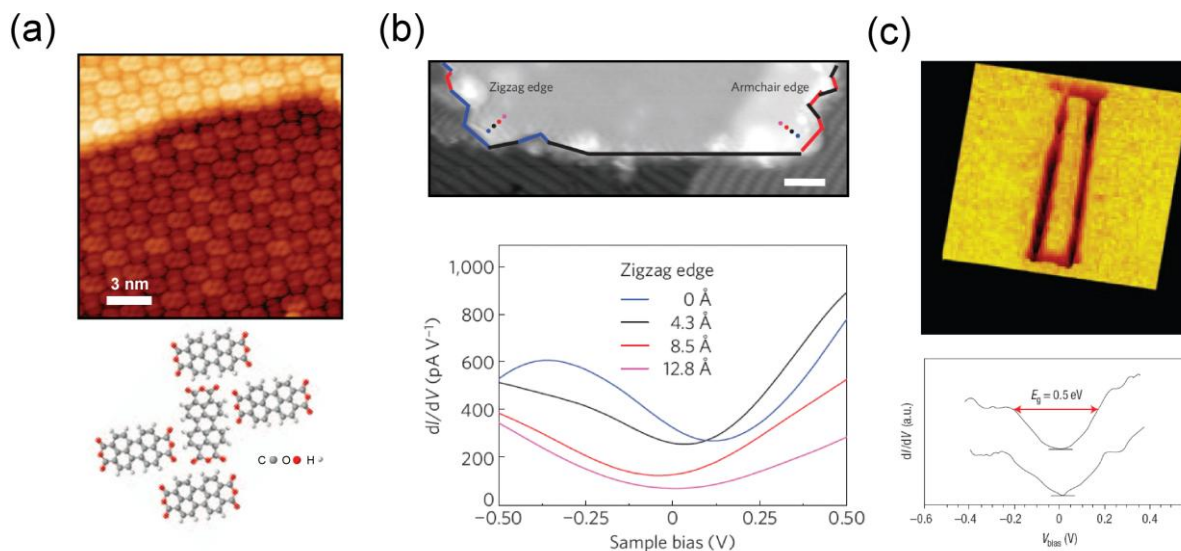


Figure. 4: STM imaging of adsorbates, edge states, and energy gaps. (a) STM image of self-assembled PTCDA on epitaxially grown graphene. The herringbone pattern and the molecular structure of PTCDA is depicted in the inset. (Adapted from Ref. [23].) (b) STM image of a $\approx(15 \text{ nm})^2$ graphene platelet exfoliated on a silicon substrate. STS spectra collected at the zigzag edges reveal an edge state at -300 mV bias. (Adapted from ref. [20].) (c) 10 nm wide GNR etched into the surface of graphite using STM lithography. STS spectra showing a zero-bias gap (E_g) of 0.5 eV in a 2.5 nm wide GNR. (Adapted from ref. [21].)

STM is a mature technique for imaging the surface topography of conducting samples with sub-nm height and lateral spatial resolution. The phenomenon underpinning the technique is the exponential increase in the tunneling of electrons between a biased conducting surface and an atomically sharp metallic tip in very close proximity ($<1 \text{ nm}$). By adjusting the tip-surface height to keep the current constant, one can track the corrugations in height produced by individual atoms. Since the properties of the tunneling current also depend sensitively on the local density-of-states (LDOS) underneath the tip, STM has simultaneous access to local electronic spectra which determine macroscopic transport properties such as the mobility. Spectra are obtained by measuring the current as a function of tip-sample bias in scanning tunneling spectroscopy (STS) mode. While graphite has a well established history with STM due to its wide availability and the ease of preparing atomically flat surfaces, obtaining STM images of graphene has required considerably more attention to surface preparation. In particular it was found that the surface must be cleaned in order to image the honeycomb lattice with atomic resolution [31,37]. Careful tip preparation (electrochemical [20] or mechanical [21] etching) has also been essential for obtaining reliable STS data. Avoiding damage to the STM tip by crashes with the surface is difficult when locating micron-sized graphene flakes, particularly on non-conducting substrates such as SiO_2 . An effective solution is to deposit a metallic film around [38] or under [34] the flake. This solution is limited however as it does not allow any comparison with bulk magnetotransport measurements and their explanation in terms of the underlying microstructure. In addition the deposition of metal films can also expose the graphene surface to unwanted chemical residues, though this

problem can be avoided by using a stencil mask or employing a post-fabrication cleaning routine [19,39]. Alternatives to this method include applying the STM to the partially suspended graphene flakes remaining on cleaved HOPG [32], or using *in situ* scanning electron microscopy for manual alignment of the tip with the flake [31].

So far atomically resolved STM images have been obtained of graphene supported by a range of different substrates (HOPG [32,33], gold [34], Ruthenium [35,36], SiC [46], SiO₂[18,19,38,43,45]) in both ambient and low temperature conditions. STM images of graphitized SiC revealed the presence of in-plane atomic defects responsible for the weak localization observed in SiC samples [46]. By contrast, STM images of SiO₂ supported graphene, which does not usually exhibit weak localization, confirmed the anticipated low density (<1 in 10⁵) [43] of defects and dislocations in exfoliated flakes [38]. Using STS to locally map the Dirac point, Deshpande *et al.* and Zhang *et al.* also compared the local curvature of exfoliated graphene with the potential landscape [18,19]. They found little correlation between the two, contrary to the idea that corrugations are the primary source of potential fluctuations responsible for electron-hole puddles at the charge neutrality point. STM studies of supported graphene invariably report the presence of out-of-plane corrugations, ranging from 0.2 nm-1 nm in height and 10 nm-30 nm in lateral dimension. Such ripples are thought to arise partly from the graphene conforming to the underlying roughness in the substrate and partly due to intrinsic rippling [31,43,45], but their contribution to scattering is still debated. Figure 2(a) shows an STM image of the self-assembly of an organic semiconductor (PTCDA) formed on epitaxially grown graphene [23]. Access to information at this scale is of particular interest in the GRAND project as a derivative of this molecule (PCDA) was used to functionalize graphene for the atomic layer deposition of Al₂O₃ [42]. The first evidence for edge states, which manifest as peaks in the STS spectra, was also obtained by STM of monoatomic step edges on the surface of bulk graphite [40,41].

Considering its merits and the overall objective of GRAND, STM is undoubtedly the tool of choice for characterising GNRs because it allows the detection of edge states and adsorbed functional groups, both of which will have a great impact on the transport properties of GNR devices. In comparison to mesoscopic 2D graphene, however, which has a relatively large surface area exposed for study, the application of STM to electrically contacted GNR devices is experimentally more challenging. To date there is no published STM study of SiO₂ supported GNRs. Several STM studies examining graphene nanostructures on conducting Si and HOPG do however offer some insight into the prospects of such a study [20,21]. Using *in situ* exfoliation of HOPG to produce nanometre-sized platelets and nanoribbons, for example, Ritter and Lyding [20] were able to identify armchair and zigzag edges [Fig. 2(b)]. Using STS they were also able to detect edge states near zigzag edges only, confirming theoretical predictions [see Fig.4(b)]. In a similar study, Tapasztó *et al.* used STM tip to etch through single atomic layers on HOPG. Figure 4(c) shows a 10 nm wide GNR etched by this method. The accompanying STS spectrum of the GNR shows a region of suppressed conductance around zero-bias, indicating the presence of a confinement gap. Providing we are able to overcome the current experimental challenges with imaging GNRs using STM our intention is to conduct the same measurements of edge states and energy gaps on GNR devices.

C. Electrostatic force microscopy

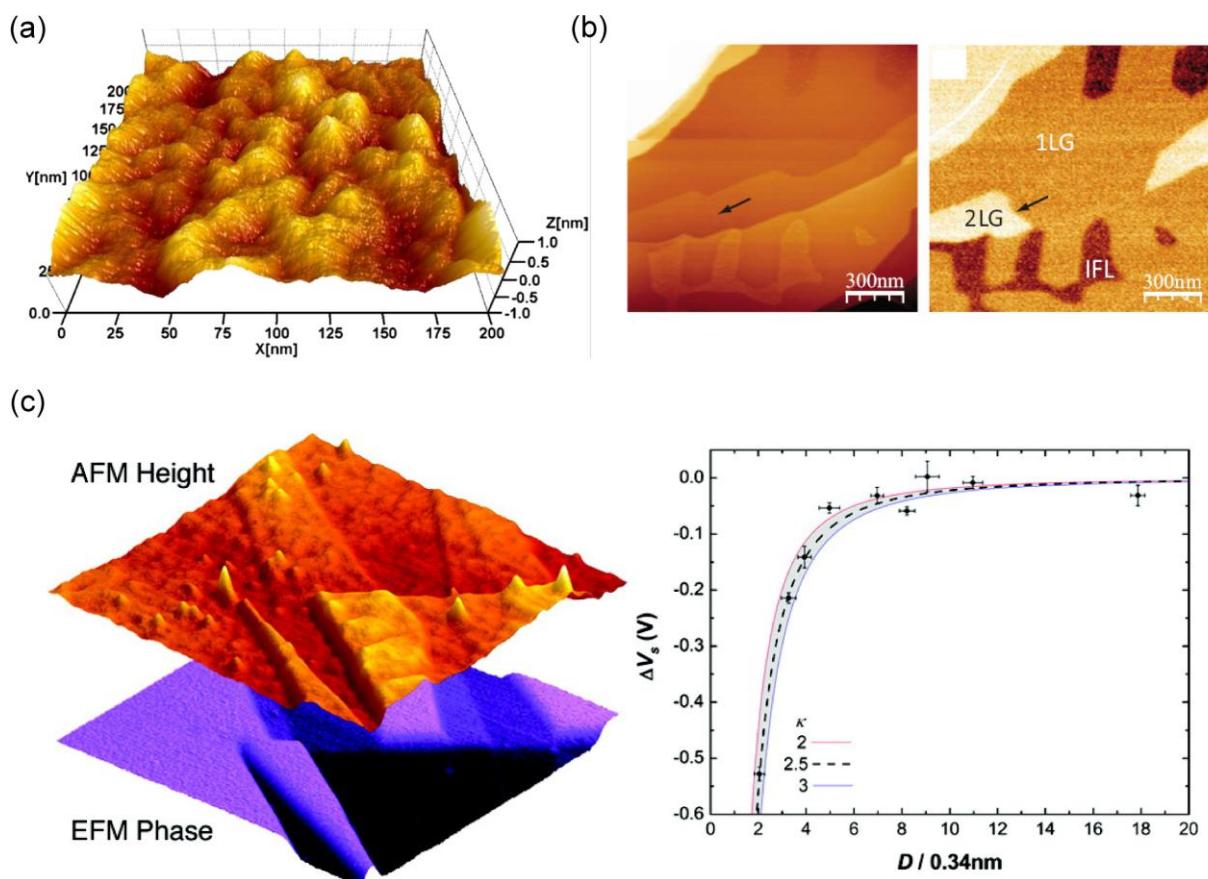


Figure. 4: Electrostatic force microscopy. (a) Typical AFM image of exfoliated graphene on SiO₂. (Adapted from ref. [45].) (b) AFM image (left) showing topography and KPM image (right) showing contact potential of graphitized SiC. Note the large change in KPM contrast associated with 2LG even though it is barely visible in the topography. (Adapted from ref. [24].) (c) [Left] 3D rendering of topography and EFM phase of graphene on SiO₂. [Right] Surface potential (ΔV) as a function of graphene thickness (D). Thicker graphene sheets screen the surface potential from the substrate more efficiently. (Adapted from ref. [6].)

EFM and KPM are scanning force microscopy (SFM) techniques used to measure stray surface electric fields with modest spatial resolution (<100 nm) and millivolt sensitivity. They provide access to the local work function of single- and few-layer graphene on different substrates [6,24], the screening and accumulation of charge due to the electric field from local gates [2], and the static electric fields due to adsorbed charges or multipoles [25] (see Fig. 1). These techniques are thus more suited to detecting spatial variations in the electrostatic environment and the many body properties of the electron sea, rather than directly probing the single particle DOS like STM.

Many of the operating principles behind EFM and KPM are well established from SFM and we provide only a brief introduction to them here. In SFM a microfabricated cantilever (typically 100 μm long) is mechanically or electrostatically excited at a frequency f_m and the deflection of its free end is measured using optical or electrical readout. The cantilever is brought within

a few hundred nanometres of the surface under investigation and a feedback circuit is used to detect the change in the cantilever's resonant frequency and oscillation amplitude due to the additional surface forces acting on the tip. Although the whole cantilever is affected by the surface, the sharp tip (10 nm radius) at its free end makes the oscillation particularly sensitive to the properties of the nanometre-sized region of the sample just underneath the tip. Far from a surface (>100 nm) the resonant frequency is constant and simply given by $f_0 = (k/m)^{1/2}$, where k is the spring constant and m is the effective mass of the cantilever, but closer to the surface the force F on the tip causes a shift in the resonant frequency given by $\Delta f = f_0/2k(dF/dz)$.

Since the measured frequency shift depends simultaneously on the tip-sample height and the surface force it can be operated in one of two distinct modes distinguished by the range of force, i.e., short- or long-range, which dominates the frequency shift. By far the most well known mode of operation is atomic force microscopy (AFM). In AFM the tip is brought into intimate (<1 nm) "contact" with the surface such that short-range Van der Waals and hard sphere repulsion are dominant. In this "tapping" mode, the frequency shift is used as the error signal of a feedback loop which adjusts the sample height to maintain a constant frequency shift ("constant force gradient") as the cantilever is scanned over the surface, allowing maps of the surface topography to be generated with atomic resolution. A typical AFM image of exfoliated graphene with sub-nm height and nm lateral resolution is shown in Fig. 5(a).

Alternatively one can focus on the shift in frequency due to spatial variations of the long-range forces, when the technique is known as frequency modulation EFM (FM-EFM). In practice EFM is performed using a "dual-pass" protocol: (i) in the first pass the surface topography $z(x, y)$ is recorded in tapping mode (ii) in the second pass the tip is withdrawn from the surface by a given distance z_0 (≈ 50 nm) and the map of the topography is used to keep the tip at a fixed distance from the surface ($z(x,y)+z_0$) while measuring Δf as a function of tip position ("constant height".) At this distance from the surface interatomic forces are negligible and the local force F between tip and sample is dominated by long-range electrostatic forces such as the capacitive force and the Coulomb interaction with surface charges under the tip. The lateral resolution of EFM inevitably suffers due to increased tip-surface separation, reducing to around 20 nm. It can be shown that to first order Δf depends quadratically on the potential difference $\Delta V = \Phi + V_S + V_T$ between the tip and the sample, where V_S is the sample voltage, V_T the tip voltage, and Φ the contact potential difference. Thus by sweeping the sample or the tip voltage it is possible to find the nulling voltage, when $\Delta V = 0$ ($V_S + V_T = -\Phi$), allowing Φ to be measured at each point on the surface. In KPM the nulling voltage is applied directly to the sample during the second pass and maps of $\Phi(x, y)$ can thus be generated in real time [24]. Fig. 4(b) shows an example of such interleaved AFM and KPM images of graphene films epitaxially grown on the silicon terminated 6H-SiC(0001) surface. Here the different work functions of single (1L) and bilayer (2L) graphene lead to a pronounced contrast in the KPM image despite only sub-nm changes in AFM height. Within GRAND KPM could prove a powerful characterisation tool for graphene produced by CEA-LETI.

As discussed earlier, structural deformations and the electrostatic environment of graphene are expected to play a key role in scattering [9]. AFM/EFM/KPM is thus a particularly important tool for diagnosing the effect of scattering due to ripples and charged impurities. Moser et al. [7], for example, were the first to use electrostatic force spectroscopy to measure

the nulling voltage at the surface of SiO_2 contaminated by adhesive residues and found a shift of the surface potential to positive values [7]. Such surface potentials may account for the shift in the neutrality point and low mobility of as-deposited flakes. Note that, while the surface force is commonly measured via the frequency shift [44], other quantities, such as the oscillation phase or amplitude, have been used instead [6]. Figure 4(c) is reproduced from Datta *et al.* [6], which studied the ability of graphene to screen the electric field from the substrate. The voltage required to null the change in the EFM phase (lag between the drive excitation and the cantilever) decreases with increasing graphene thickness, demonstrating that screening increases with the number of layers. These data suggest that in EFM mode it would also be possible to measure the electric field penetration from the silicon back-gate. Since GNR devices will have a gap in the density of states, and when there is a gap the screening is reduced, EFM offers another method for mapping out energy gaps in GNRs using the variation in screening of the electric field.

D. Raman

The technique of RAMAN spectroscopy is based on inelastic photon scattering with optical-coupled phonons and is a non-invasive method for analysing phonon modes in solids. Since the frequencies of phonons in graphene, in particular the frequencies of the so called G and the 2D phonon, depend on the numbers of graphene layers involved, RAMAN spectroscopy has become a standard method for determining the number of layers in graphene flakes [49]. At AMO and CAE-Leti RAMAN spectroscopy is used routinely to determine the layer number for both exfoliated graphene (AMO) and epitaxial graphene (CEA-Leti) before processing. CEA-Leti also uses RAMAN spectroscopy in combination with AFM for demonstrating graphene formation on SiC (for details see deliverable 2.2.)

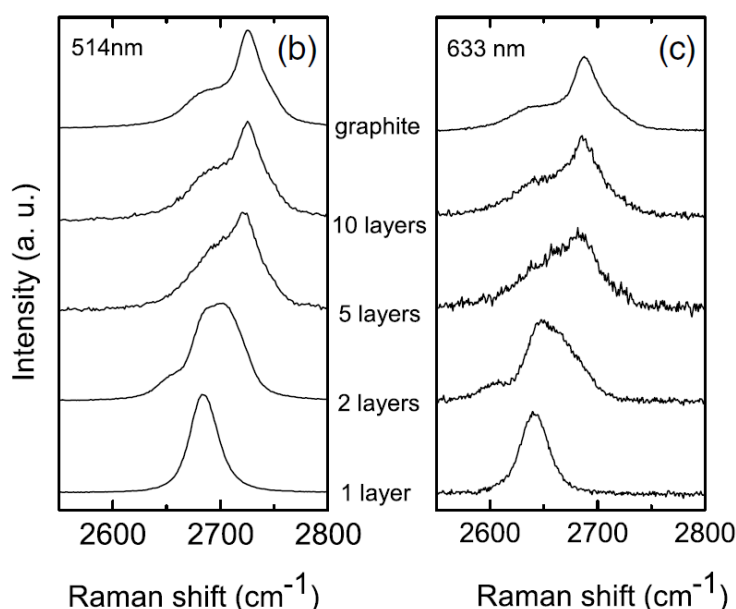


Figure 5: RAMAN spectra from graphene to bulk graphite. The spectra reduce to frequencies around the 2D peak for excitation wavelengths of (b) 514 nm (b) 633 nm (Adapted from [49]).

E. Other techniques

Other techniques such as scanning photocurrent microscopy (SPCM) [11–14], scanning single electron transistor (SET) [9], and scanning capacitance microscopy (SCM) [10], while important in the field, will not feature strongly in our nanoanalytics work. By comparison SPCM offers comparatively poor spatial resolution (about 300 nm) owing to the spot size of excitation laser. The ability to operate in ambient conditions with relatively good potential sensitivity means SPCM studies of graphene have tended to concentrate on mesoscopic fluctuations in potential due to charge transfer from metal contacts and charged surface impurities. Scanning SET is a niche low temperature (LT) technique capable of detecting microvolt fluctuations in surface potential with a spatial resolution set by the area of the SET (typically 100 nm). To date some of the most compelling evidence for electron-hole puddles has been obtained by SSET [9]. The application of SCM [26] to graphene is also in its infancy. It is unique in the sense that direct electrical contact is made between a metallic tip and the graphene, making scanning highly invasive and potentially destructive. As such rastered imaging has not been performed but point spectroscopy has allowed lengthscales of the disorder potential down to 5 nm to be inferred [10].

III. CONCLUSIONS

In conclusion we have reviewed some of the techniques currently used to image nano- and mesoscale topographic and electrostatic features in exfoliated graphene. We have demonstrated that scanning gate microscopy is capable of characterising the local density of charged impurities in 2D graphene with 50 nm resolution. We will exploit this capability in future experiments to examine the doping effect of chemical processing recipes being developed by TNI-UCC to functionalise GNRs. In addition, we measured the transport properties of a 1D GNR and showed that SGM can be used to image localised states. In future this will allow us to image the defect density in narrower GNRs manufactured by AMO. The capabilities of STM and EFM have been discussed and illustrated using images from the recent literature. Finally we have drawn on recent precedents in the literature to make the case for STM/EFM measurements of energy gaps and edge states in GNRs, and EFM/KPM for characterising graphitised SiC grown by CEA-LETI.

IV. REFERENCES

- [1] J. Sabio, C. Seonez, S. Fratini, F. Guinea, A. H. C. Neto, , and F. Sols, *Phys. Rev. B* 77, 195409 (2008).
- [2] N. J. Lee, J. W. Yoo, Y. J. Choi, C. J. Kang, D. Y. Jeon, D. C. Kim, S. Seo, and H. J. Chung, *Appl. Phys. Lett.* 95, 222107 (2009).
- [3] Y.-J. Yu, Y. Zhao, S. Ryu, L. E. Brus, K. S. Kim, and P. Kim, *Nano Lett.* 9, 3430 (2009).
- [4] M. R. Connolly, K. L. Chiou, C. G. Smith, D. Anderson, G. A. C. Jones, A. Lombardo, A. Fasoli, and A. C. Ferrari, *arXiv:0911.3832v2* (2009).
- [5] J. Berezovsky and R. M. Westervelt, *arXiv:0907.0428v1* (2009).
- [6] S. S. Datta, D. R. Strachan, E. J. Mele, and A. T. C. Johnson, *Nano Letters* 9, 7 (2009).
- [7] J. Moser, A. Verdaguer, D. Jimenez, A. Barreiro, and A. Bachtold, *Appl. Phys. Lett.* 92, 123507 (2008).
- [8] A. Verdaguer, M. Cardellach, J. J. Segura, G. M. Sacha, J. Moser, M. Zdrojek, A. Bachtold, and J. Fraxedas, *Appl. Phys. Lett.* 94, 233105 (2009).
- [9] J. Martin, N. Akerman, G. Ulbricht, T. Lohmann, J. Smet, K. V. Klitzing, and A. Yacoby,

Nature physics 4, 144 (2008).

[10] F. Giannazzo, S. Sonde, V. Raineri, and E. Rimini, Nano Letters 9, 23 (2009).

[11] E. J. H. Lee, K. Balusubramanian, R. T. Weitz, M. Burghard, and K. Kern, Nature Nanotechnology 3, 486 (2008).

[12] T. Mueller, F. Xia, M. Freitag, J. Tsang, and P. Avouris, Phys. Rev. B. 79, 245430 (2009).

[13] F. Xia, T. Mueller, R. Golizadeh-Mojarad, M. Freitag, Y. ming Lin, J. Tsang, V. Perebeinos, and P. Avouris, Nano Letters 9, 1039 (2009).

[14] R. S. Sundaram, C. Gomez-Navarro, E. J. H. Lee, M. Burghard, and K. Kern, Appl. Phys. Lett. 95, 223507 (2009).

[15] M. Freitag, M. Steiner, Y. Martin, V. Perebeinos, Z. Chen, J. C. Tsang, and P. Avouris, Nano Lett. 9, 1883 (2009).

[16] C. Stampfer, F. Molitor, D. Graf, K. Ensslin, A. Jungen, C. Hierold, and L. Wirtz, Appl. Phys. Lett. 91, 241907 (2007).

[17] Z. H. Ni, T. Yu, Z. Qiang, Y. Y. Wang, L. Liu, C. P. Wong, J. Miao, W. Huang, and Z. X. Shen, ACS Nano 3, 569 (2009).

[18] A. Deshpande, W. Bao, F. Miao, C. N. Lau, and B. J. LeRoy, Phys. Rev. B 79, 205411 (2009).

[19] Y. Zhang, V. W. Brar, C. Girit, A. Zettl, and M. F. Crommie, Nature Physics 5, 722 (2009).

[20] K. A. Ritter and J. W. Lyding, Nature Materials 8, 235 (2009).

[21] L. Tapasztó, G. Dobrik, P. Lambin, and L. P. Biro, Nature Nanotechnology 3, 397 (2008).

[22] P. Lauffer, K. V. Emtsev, R. Graupner, T. Seyller, and L. Ley, phys. stat. sol(b) 10, 2064 (2008).

[23] Q. H. Wang, M. C. Hersam, Nature Chemistry, 1, 206 (2009).

[24] T. Filleter, K. V. Emtsev, T. Seyller, and R. Bennewitz, Appl. Phys. Lett. 93, 133117 (2008).

[25] L. Chen, R. Ludeke, X. Cui, A. G. Schrott, C. R. Kagan, and L. E. Brus, J. Phys. Chem. B 109, 1834 (2005).

[26] D. T. Lee, J. P. Pelz, and B. Bhushan, Rev. Sci. Instr. 73, 3525 (2002).

[27] M. Y. Han, B. Ozyilmaz, Y. Zhang, and P. Kim, Phys. Rev. Lett 98, 206805 (2007).

[28] F. Molitor, A. Jacobsen, C. Stampfer, J. Guttinger, T. Ihn, and K. Ensslin, Phys. Rev. B 79, 11, 075426 (2009).

[29] K. Todd, H.-T. Chou, S. Amasha, and D. Goldhaber-Gordon, Nano Letters 9, 416 (2009).

[30] H. E. Romero, N. Shen, P. Joshi, H. R. Gutierrez, S. A. Tadigadapa, J. O. Sofo, and P. C. Eklund, ACS Nano 2, 2037 (2008).

[31] M. Ishigami, J. H. Chen, W. G. Cullen, M. S. Fuhrer, and E. D. Williams, Nano Letters 7, 1643 (2007).

[32] A. Luican, G. Li, and E. Y. Andrei, Solid State Communications 149, 1151 (2009).

[33] A. L. Guohong Li and E. Y. Andrei, Phys. Rev. Lett. 102, 176804 (2009).

[34] Z. Klusek, P. Dabrowski, P. Kowalczyk, W. Kozłowski, W. Olejniczak, P. Blake, M. Szybowski, and T. Runka, Appl. Phys. Lett 95, 113114 (2009).

[35] J. T. S. E. Sutter, D. P. Acharya and P. Sutter, Appl. Phys. Lett. 94, 133101 (2009).

[36] A. L. V. de Parga, F. Calleja, B. Borca, J. M. C. G. Passeggi, J. J. Hinarejos, F. Guinea, and R. Miranda, Phys. Rev. Lett. 100, 056807 (2008).

[37] E. Stolyarova, D. Stolyarov, L. Liu, K. T. Rim, Y. Zhang, M. Han, M. Hybersten, P. Kim, and G. Flynn, J. Phys. Chem. C 112, 6681 (2008).

[38] E. Stolyarova, K. T. Rim, S. Ryu, J. Maultzsch, P. Kim, L. E. Brus, T. F. Heinz, M. S. Hybertsen, and G. W. Flynn, PNAS 104, 9209 (2007).

[39] Y. Shi, W. Fang, K. Zhang, W. Zhang, and L.-J. Li, small 95, 222107 (2009).

[40] Y. Kobayashi, K. ichi Fukui, T. Enoki, K. Kusakabe, and Y. Kaburagi, Phys. Rev. B 71, 193406 (2005).

[41] Y. Niimi, T. Matsui, H. Kambara, K. Tagami, M. Tsukada, and H. Fukuyama, Phys. Rev. B 73, 085421 (2006).

[42] X. Wang, S. M. Tabakman, and H. Dai, J. Am. Chem. Soc. 130, 8152 (2008).

[43] K. Xu, P. Cao, and J. R. Heath, Nano Lett. 104, 18392 (2009).

- [44] Y. Lu, M. Munoz, C. S. Steplecaru, C. Hao, M. Bai, N. Garcia, K. Schindler, and P. Esquinazi, *Phys. Rev. Lett* 97, 076805 (2006).
- [45] V. Geringer, M. Liebmann, T. Echtermeyer, S. Runte, M. Schmidt, R. Ruckamp, M. C. Lemme, and M. Morgenstern, *Phys. Rev. Lett* 102, 076102 (2009).
- [46] G. M. Rutter, J. N. Crain, N. P. Guisinger, T. Li, P. N. First, and J. A. Stroscio, *Science* 317, 219 (2007).
- [47] S. Adam, S. Cho, M. S. Fuhrer, , and S. D. Sarma, *Phys. Rev. Lett.* 101, 046404 (2008).
- [48] F. Sols, F. Guinea, and A. H. C. Neto, *Phys. Rev. Lett.* 99, 166803 (2007).
- [49] Ferrari *et al.* *Phys. Rev. Lett.* 97,187401 (2006).